MRI-based Delta-Radiomic Features for Prediction of Local Control in Liver Lesions Treated with Stereotactic Body Radiation Therapy

Will H Jin (willhjin@gmail.com)
Jackson Memorial Hospital
Garrett N Simpson
University of Miami, University of Miami
Nesrin Dogan
University of Miami, University of Miami
Benjamin Spieler
University of Miami, University of Miami
Lorraine Portelance
University of Miami, University of Miami
Fei Yang
University of Miami, University of Miami
John C Ford
University of Miami, University of Miami

Article

Keywords: delta radiomics, radiomics, SBRT, texture features, MRI-guided

Posted Date: May 18th, 2022

DOI: https://doi.org/10.21203/rs.3.rs-1623594/v1

Abstract

Purpose/Objectives: Real-time magnetic resonance image guided stereotactic ablative radiotherapy (MRgSBRT) is used to treat abdominal tumors. Longitudinal data is generated from daily setup images. Our study aimed to identify delta radiomic texture features extracted from these images to predict for local control in patients with liver tumors treated with MRgSBRT.

Materials/Methods: Retrospective analysis of an IRB-approved database identified patients treated with MRgSBRT for primary liver and secondary metastasis histologies. Daily low field strength (0.35 T) images were retrieved, and the gross tumor volume was identified on each image. Next, images' gray levels were equalized, and 39 second-order texture features were extracted. Delta-radiomics were calculated as the difference between feature values on the initial scan and after delivered biological effective doses (BED, $\alpha/\beta = 10$) of 20 Gy and 40 Gy. Then, features were ranked by the Gini Index during training of a random forest model. Finally, the area under the receiver operating characteristic curve (AUC) was estimated using a bootstrapped logistic regression with the top two features.

Results: We identified 22 patients for analysis. The median dose delivered was 50 Gy in 5 fractions. The top two features identified after delivery of BED 20 Gy (1 fraction) were gray level co-occurrence matrix features energy and gray level size zone matrix based large zone emphasis. The model generated an AUC = 0.9011 (0.752–1.0) during bootstrapped logistic regression. The same two features were selected after delivery of a BED 40 Gy, with an AUC = 0.716 (0.600–0.786).

Conclusions: Delta-radiomic features after a single fraction of SBRT predicted local control in this exploratory cohort. If confirmed in larger studies, these features may identify patients with radioresistant disease and provide an opportunity for physicians to alter management much sooner than standard restaging after 3 months. Expansion of the patient database is warranted for further analysis of delta-radiomic features.

Background

Stereotactic body radiation therapy (SBRT) is an established treatment option for both primary hepatocellular carcinoma (HCC) and metastatic lesions within the liver [1–4]. In primary HCC, Magnetic resonance guided (MRg) linear accelerators (linacs) is being explored as a complementary tool to support the patient prior to definitive hepatectomy or transplant. Without definitive resection, 5-year overall survival is estimated at less than 10% [5]. Improving progression free survival acts to bridge patients until definitive treatment, another line of chemotherapy or in the palliative setting. In liver metastases, it offers a safe and convenient way to obtain durable local control for metastasis-directed therapies (MDT) [6–8]. MRgSBRT provide an ideal platform for treating abdominal lesions due to its distinct advantages over standard-of-care cone beam computerized tomography (CBCT) image guidance. First, the superior soft tissue visualization [9] of MR images eliminates the need for fiducial marker placement required for localizing oncologic targets in CBCT imaging. Second, MRg linacs provide real-time tracking during

treatment with automatic beam control. Motion management remains a challenge in abdominal tumors due to the proximity to the diaphragm, and this feature automatically turns off the beam when the target is out of range. Third, there is no unnecessary ionizing radiation delivered when daily imaging is done on the MR system. Finally, a fourth, yet unquantified benefit may come from analyzing the imaging data generated from daily image-guidance.

Despite low field strengths, the images generated from daily MR set up images have adequate soft tissue contrast to visualize targets and organs at risk (OAR). During the last decade, the field of oncology moved towards personalized medicine[9], and radiomics presented itself as a pathway for imaging to potentially guide personalized management decisions. Radiomics texture analysis quantifies the spatial relationships of individual voxel characteristics within a region of interest [10]. These statistical descriptors served as imaging biomarkers used in models for predicting toxicities, risk stratification, and oncologic outcomes [11–18]. Baseline MR characteristics of different liver lesions are heterogeneous and present a challenge for texture analysis. For example, on non-enhanced T2 weighted imaging, liver metastases may appear as central regions of hypointense necroses surrounded by hyperintense rims of viable tumor. Whereas primary HCC may present as a heterogeneous, mixed signal lesion and intrahepatic cholangiocarcinomas (ICC) may appear as hyperintense lesions. Despite these heterogeneous presentations, delta radiomics may be able to discern a meaningful signal, as it only examines changes between the baseline and subsequent images.

Delta-radiomics expands upon texture analysis by considering changes in features induced by treatments. Delta-radiomics is gaining traction and initial studies seem promising. Fave et al initially postulated that predictive information can be extracted from CBCT set up images in lung cancer patients [19], while Boldrini et al applied this concept to low field strength MR setup images and correlated delta-radiomics texture values with response to neoadjuvant therapy in rectal cancer patients [20]. Neoadjuvant therapy consists of combination chemoradiation, with the goal to shrink tumors as much as possible for a potential surgery. In the setting of SBRT, we suspect that changes in texture features proxy different responses to radiation. By extracting features from multiple timepoints, phenotypic changes in the tumor microenvironment during treatment can be captured and used for predictive modelling [16,21]. We hypothesize two theoretical strengths with delta-radiomics. First, data required for analysis is readily available since it comes directly from MRgSBRT. Secondly, one can potentially predict for treatment response much sooner than with standard of care imaging protocols. Treatment response is normally evaluated at least three months after treatment via Response Evaluation Criteria in Solid Tumors (RECIST) or modified RECIST (mRECIST) [22]. These grading systems primarily rely on size of index lesions or intensity of metabolic imaging. This much time is needed to allow for adequate resolution of non-pathologic inflammatory changes incurred from ablative radiation. If treatment response were available immediately at the end of treatment, clinicians potentially gain valuable time to adjust management strategies like coordinating other MDT for liver metastases or chemotherapies for primary HCC.

The purpose of this work is to identify delta-radiomics texture features computed as a function of biological effective dose (BED) that could serve as predictive markers for local control in liver lesions treated with MRgSBRT. We hypothesize that the most meaningful delta-radiomics features will be identified earlier versus later during treatment and that a combined clinical-radiomics model will perform better than a radiomics or clinical model alone.

Methods

Patient Selection

Retrospective analysis of an IRB-approved database of patients treated on our MRg system was done to identify patients with liver lesions treated with MRgSBRT. Patients were included if they had a biopsy-proven primary HCC, known history of a primary malignancy with biopsy-proven metastasis, or consensus to treat after review in a multidisciplinary tumor board. Patients were excluded from analysis if they had synchronous primary malignancies, did not complete MRgSBRT, or did not have post-treatment imaging for restaging. Data abstracted included demographics, performance status, history of cirrhosis, history of hepatitis C infection, prior radiofrequency ablations, prior radiation treatments, prior chemotherapy regimens, prior trans-arterial chemoembolization procedures, pre-treatment complete metabolic panels, pre-treatment complete blood counts, tumor size, tumor location in the liver, histology, radiation dose delivered, and radiation fractions delivered.

Image Acquisition and Target Delineation

Low field strength setup MR images acquired on a 0.35 T split bore unit using a balanced steady-state free procession pulse sequence were retrieved from the MR linac treatment planning system. The image acquisition protocol was similar for all images acquired during treatment; breath-hold images were acquired in 25 seconds with voxel dimensions of 1.5 x 1.5 x 3.0 mm^3. Two torso coils with six-phased array elements were placed hemi-circumferentially around the patient. Gross Tumor Volume (GTV) was delineated by a radiation oncologist resident and reviewed by a board-certified radiation oncologist experienced in MRgSBRT and low field MR setup images. MRI safety screening were administered to all eligible patients. Treatment response of restaging scans was assessed using RECIST and mRECIST criteria, depending on initial histology.

Image Analysis, radiomic feature selection, and model construction

Image DICOM files along with the associated GTV structure sets were exported to a local drive and radiomics texture features were extracted using the Texture Analysis Toolbox in MATLAB 2020b (The MathWorks, Natick MA, USA). Binary masks of the GTVs were generated to extract three-dimensional bitmaps from the RTStruct DICOM objects. The dynamic range of intensity values was constrained via "±3σ" Collewet normalization method [23]. A total of 39 second-order features were extracted from the GTVs of the daily MR setup images. Feature classes utilized were gray level co-occurrence matrix (GLCM), gray level size zone matrix (GLSZM), gray level run length matrix (GLRLM), and neighborhood gray tone

difference matrix (NGTDM) [24–28]. The GLCM code/aggregation code for calculation of the GLCM was LFYI/IAZD with the feature name 8ZQL when using the Image Biomarker Standardization Initiative (IBSI) nomenclature [29]. The IBSI code/aggregation code for the GLSZM is 9SAK/KOBO and the feature name and formula is 48P8. Delta-radiomic texture features were calculated as the change in radiomic features between the initial setup image (before treatment) and after BEDs of 20 Gy and 40 Gy were delivered, producing BED_{20} and BED_{40} feature libraries. These quanta of radiation were selected to account for dissimilar radiation doses and fractionation schedules. For example, a delta-radiomics texture feature value calculated from a hypothetical patient with a BED/Fx = 10 Gy would be calculated for the BED_{20} with the texture features calculated from the image acquired prior to fraction 1 and the setup image from fraction 3 (delivery of 2 treatments).

Model construction and feature selection

A two-step method was used where the first step was designed to rank features in order of predictive potential, while the second step was used to evaluate the top features. In step one, features were ranked using the Gini Index, calculated during the training phase of a random forest (RF) model. The Gini Index is a measure of how important each predictive variable is for accurate prediction [30]. A RF model was built using delta-radiomics as predictors with 500 decision trees considering six features ('mtry' parameter) with replacement one at a time. The 'mtry' parameter was selected as approximately the square root of the number of delta-radiomics texture features under consideration, thirty-nine total for each timepoint. The RF prediction model selects subsets of the available data for predictors, constructs a simple decision tree, then evaluates the accuracy of predictors included and excluded from each decision tree. This is performed for each tree in the forest. The importance of the variables in the model for prediction is calculated and recorded as the Gini Index. Finally, the two features with the highest Gini Index were selected for further investigation.

Those two features were used to estimate the internal validation area under the receiver operating characteristic curve (AUC) using a bootstrapped logistic regression model. The model was bootstrapped 1,000 times randomly sampling 2/3 of the patient data at each iteration. The internal validation AUC was obtained by feeding in the remaining 1/3 of the patients and predicting response. The AUC was recorded for each iteration. This process was performed for both BED_{20} and BED_{40} features that were selected by the Gini Index. The mean AUC, 2.5 percentile, and 97.5 percentile values were calculated using the 1,000 iterations. Two additional random forest models were constructed, a strictly clinical model, and a combined model (delta-radiomic BED_{20} features with clinical data), to compare the importance of clinical variables and BED_{20} delta-radiomic texture features using the Gini Index. The clinical model included BED/fraction, maximum tumor dimension, sex, ethnicity, initial Karnofsky performance status score, and existence of prior cirrhosis as variables for predicting treatment response. The AUC estimates produced by the random forest model during training was recorded for evaluation. The process was repeated for the combined model with the top two BED_{20} delta-radiomics features included to assess the importance of the factors relevant to available clinical information. Both the clinical model and combined models

were constructed with 500 trees. The mtry parameter was set to include all data (mtry = 6 for the clinical model and mtry = 8 for the combined model).

Ethics Declaration

All methods were carried out in accordance with relevant guidelines and regulations.

The study was approved by The University of Miami's institutional IRB committee under IRB#20160817. Informed consent was waived due to the retrospective nature of the study by The University of Miami's institutional IRB.

Results

Patient and Treatment Characteristics

A total of 22 patients were identified in the database. The median age of patients was 73 years old, ranging from 49 to 94 years old (Table 1). Treatment regimens consisted of 3–5 fractions delivering physical doses of 30 Gy to 60 Gy. The median BED, calculated with an $\alpha/\beta = 10$, was 100 Gy, ranging from 48 to 180 Gy [22]. The median BED/Fx was 20 Gy with a range from 9.6 to 60 Gy/Fx. Median follow-up for the entire cohort was 13.98 months.

Table 1

Patient variables included for delta-radiomics texture analysis. BED: biologically effective dose (calculated using $\alpha/\beta = 10$), HCC: hepatocellular carcinoma, ICC: intrahepatic cholangiocarcinoma, LM: secondary liver metastases

Patient Number	Poor Treatment Response	Age (years)	Rx (Gy)	Fractions	Total BED	BED/Fx	Tumor Size in Largest Dimension (cm)	Diagnosis
1	Yes	66	45	5	85.5	17.1	4.3	HCC
2	No	62	50	5	100	20	2	LM
3	No	70	50	5	100	20	7.8	HCC
4	Yes	66	45	5	85.5	17.1	1.3	LM
5	Yes	56	50	5	100	20	3.1	LM
6	Yes	74	50	5	100	20	2.1	LM
7	No	92	50	5	100	20	7.2	HCC
8	No	81	40	4	80	20	1.8	LM
9	No	75	50	5	100	20	3.9	HCC
10	No	79	50	5	100	20	4.3	ICC
11	No	70	50	5	100	20	2.7	HCC
12	No	90	50	5	100	20	6.4	HCC
13	Yes	49	30	5	48	9.6	8	LM
14	No	84	50	5	100	20	7.3	LM
15	No	54	50	5	100	20	2.5	HCC
16	Yes	72	60	5	132	26.4	2.4	LM
17	No	87	54	3	151.2	50.4	1.8	LM
18	No	59	30	3	60	20	2.7	HCC
19	Yes	50	50	5	100	20	4.8	LM
20	No	94	60	3	180	60	1.7	LM
21	No	94	60	3	180	60	1.7	LM
22	No	91	50	5	100	20	4.7	ICC

Delta Radiomics Feature Selection

The two features selected for the BED_{20} library were gray level co-occurrence matrix (GLCM) energy and gray level size zone matrix (GLSZM) based large zone emphasis. During model training, the estimated AUC for the BED_{20} delta-radiomics features was 0.920 (Fig. 1). Based on the selected delta-radiomics BED_{20} features, the bootstrapped logistic regression achieved a mean AUC = 0.901 with the 2.5 percentile – 97.5 percentile range = 0.752–1.0 (Table 2). The BED_{40} delta-radiomic texture feature model selected the same two features but calculated a higher Gini Index for gray level size zone matrix (GLSZM) large zone emphasis than for energy (GLCM). During model training, the estimated AUC for the BED_{40} delta-radiomics features was 0.638 (Fig. 1). The bootstrapped logistic regression resulted in an AUC = 0.716 with the 2.5 to 97.5 percentile range = 0.600 to 0.786 using the selected BED_{40} delta-radiomic texture features (Table 2).

Table 2
Performance of delta-radiomics texture features ranked by the Gini Index using bootstrapped logistic regression analysis for each library. AUC: area under the curve, BED: biologically effective dose (calculated using $\alpha/\beta = 10$).

Delta-radiomics library	Highest Gini Index Feature	Second Highest Gini Index Feature	Mean AUC	2.5 Percentile Value	97.5 Percentile Value
BED_{20}	Energy	Large Zone Emphasis	0.901	0.752	1.0
BED_{40}	Large Zone Emphasis	Energ	0.716	0.600	0.786

Combined Clinico-radiomics Modeling

For clinical features, the random forest model selected maximum tumor dimension as most important, closely followed by BED/fraction. The model estimated the AUC = 0.724 with 95% confidence interval = 0.446–1.0. The combined model ranked GLCM energy as most important for predictive accuracy, followed by GLSZM large zone emphasis, then tumor size, and BED/fraction. The inclusion of the BED20 delta-radiomics texture features to the clinical model improved the performance estimation with an AUC = 0.895 with the 95% confidence interval = 0.762–1.0.

Discussion

To our knowledge, this is the first study evaluating delta-radiomic features of daily adaptive MR imaging in liver lesions treated with SBRT. Two features, GLCM energy and GLSZM large zone emphasis, were identified that could predict local control. Features identified earlier in treatment (BED_{20}) performed better than those using features later (BED_{40}) in treatment. Interestingly, the combined clinico-radiomics model did not perform better than the BED_{20} model alone. If validated in prospective studies, delta-radiomics could drastically reduce the time clinicians need to make critical changes in management decisions. In primary HCC, early detection of poor responsivity to radiation can give clinicians enough time to prepare additional bridging therapies. In metastatic cases, delta-radiomics may provide an assurance to switch

lines of systemic therapy. The earlier we can detect an actionable signal among the noise, the more benefit we provide to our patients.

Other studies reported different features and varying optimal times for evaluating such features. Gemelli University produced two series of adaptive delta radiomics studies on a 0.35 T on-board MR-linac, in a collaboration with University of Wisconsin. In their LARC cohort, they were able to predict pCR using two radiomic features, L_{least} and glnu [31,32]. In their locally advanced pancreatic cancer cohort, texture features like GLCM, GLRLM, and GLDZM predicted for crude 1-year local control with an AUC of 0.79 [33]. These texture features were predictive of local control after BED_{40Gy} was delivered, equivalent to a complete course of 5 fractions. Most prior studies evaluated the utility of delta features between pre- and post-treatment images. In MRgSBRT for pancreatic cancer, Simpson et al [34] suggested that delta-radiomics texture features could be predictive of local control after the first fraction as well. Including this current study, GLCM energy was associated with treatment response in three different histologies [34,35].

In this study, GLCM energy and GLSZM large zone emphasis were identified as predictive features for treatment response. Features identified earlier in treatment produced a stronger predictive signal than features later in treatment. These features increased in patients who responded to treatment between the beginning of treatment and delivery of 20 Gy BED (Fig. 2). Delivery of another 20 Gy BED resulted in a decrease in feature values between the 20 Gy BED and 40 Gy BED timepoints. Patients with no treatment response demonstrated opposite trends, with an initial decrease in feature values followed by an increase by the 40 Gy BED point. This suggests that a key event for SBRT cell killing occurs with the first treatment with diminishing returns. The premise for texture-based delta radiomics is based on the hypothesis that phenotype is a proxy for biologic behavior. GLCM energy appears to be an interesting feature identified across multiple histologies that could predict for SBRT response. We hypothesize this may be due to vascular endothelial damage and reactive acute inflammation, but correlative radiobiology studies will need to confirm the architectural changes

There are several shortcomings to this exploratory work. Generalizability and reproducibility were limited by the number of patients enrolled and the heterogeneity of the cohort. Subgroup analysis based on histology was not possible due to lack of sufficient statistical power and will need to be clarified prior to making conclusions regarding clinical management. Only second order texture features were included in this analysis for calculation of delta-radiomics texture analysis because of interpretability and generalizability. Many higher order texture features include complicated image filtering and meaningful data can be obscured from investigators [36,37]. Additionally, second order texture features are included in most texture analysis studies with an established literature across many modalities and disease sites [38–42]. Finally, other texture features were excluded to increase the specificity of variables *a priori*, given the small cohort. Also, as in all radiomics texture analysis studies, results could be impacted by contouring variability. GTV contouring is a relatively subjective task and future studies need to develop a generalizable, regimented protocol for delineating GTVs on images or automated contouring algorithms could help mitigate variability. Generalizability and reproducibility were limited by the number of patients

enrolled and the heterogeneity of the cohort. Lastly, the binary nature of the response and use of RECIST 1.1 could smooth over the response data, and future analysis should aim to include measurable or observable biology for response determination.

Conclusion

This preliminary MR-based delta-radiomics texture analysis study suggests that low field MR setup images may be able to capture meaningful phenotypic data, reflective of biologic changes seen as treatment response to SBRT. It may be possible, with expanded studies, to identify patients with liver malignancies treated with MRgSBRT at high risk for poor treatment response. The ability to identify non-responders prior to standard restaging scans three months after SBRT should not be understated and rigorously explored moving forward. Further work will be undertaken to include an expanded patient library and an external validation cohort, potentially leading to multi-institutional studies.

Declarations

Author contributions

WJ wrote the main manuscript text. GS performed the statistical analysis and prepared all figures. ND, BS, LP, FY, and JCF assisted with project conception and study design. All authors contributed to manuscript review and editing.

Competing Interests

All authors have no conflicts of interest to declare.

Data Availability

The datasets generate during and/or analyzed during the current study are available from the corresponding author on reasonable request.

References

1. Wulf, J. *et al.* Stereotactic radiotherapy of targets in the lung and liver. Strahlentherapie und Onkologie **177**, 645–655, doi:10.1007/PL00002379 (2001).
2. Bujold, A. *et al.* Sequential phase I and II trials of stereotactic body radiotherapy for locally advanced hepatocellular carcinoma. J. Clin. Oncol. **31**, 1631–1639, doi:10.1200/JCO.2012.44.1659 (2013).
3. Tse, R. V. *et al.* Phase I study of individualized stereotactic body radiotherapy for hepatocellular carcinoma and intrahepatic cholangiocarcinoma. J. Clin. Oncol. **26**, 657–664, doi:10.1200/JCO.2007.14.3529 (2008).
4. Rosenberg, S. A. *et al.* A Multi-Institutional Experience of MR-Guided Liver Stereotactic Body Radiation Therapy. Adv Radiat Oncol **4**, 142–149, doi:10.1016/j.adro.2018.08.005 (2019).

5. Sharma, R. Descriptive epidemiology of incidence and mortality of primary liver cancer in 185 countries: evidence from GLOBOCAN 2018. Jpn J Clin Oncol **50**, 1370–1379, doi:10.1093/jjco/hyaa130 (2020).
6. Schefter, T. E. *et al.* A phase I trial of stereotactic body radiation therapy (SBRT) for liver metastases. Int J Radiat Oncol Biol Phys **62**, 1371–1378, doi:10.1016/j.ijrobp.2005.01.002 (2005).
7. Dawson, L. A., Eccles, C. & Craig, T. Individualized image guided iso-NTCP based liver cancer SBRT. Acta Oncol **45**, 856–864, doi:10.1080/02841860600936369 (2006).
8. Tse, R. V. *et al.* Phase I study of individualized stereotactic body radiotherapy for hepatocellular carcinoma and intrahepatic cholangiocarcinoma. J Clin Oncol **26**, 657–664, doi:10.1200/JCO.2007.14.3529 (2008).
9. Hood, L. & Friend, S. H. Predictive, personalized, preventive, participatory (P4) cancer medicine. Nature Reviews Clinical Oncology **8**, 184–187, doi:10.1038/nrclinonc.2010.227 (2011).
10. Castellano, G., Bonilha, L., Li, L. M. & Cendes, F. Texture analysis of medical images. Clinical Radiology **59**, 1061–1069, doi:http://dx.doi.org/10.1016/j.crad.2004.07.008 (2004).
11. Lewis, S., Hectors, S. & Taouli, B. Radiomics of hepatocellular carcinoma. Abdom. Radiol., doi:10.1007/s00261-019-02378-5 (2020).
12. Green, M. *et al.* Radiomic Features Predict Esophagitis Risk in Non-Small Cell Lung Cancer Patients Treated with Radiation. International Journal of Radiation Oncology • Biology • Physics **99**, S14, doi:10.1016/j.ijrobp.2017.06.049.
13. Wang, G. *et al.* Pretreatment MR imaging radiomics signatures for response prediction to induction chemotherapy in patients with nasopharyngeal carcinoma. European Journal of Radiology **98**, 100–106, doi:10.1016/j.ejrad.2017.11.007 (2018).
14. Abdollahi, H. *et al.* MRI Radiomic Analysis of IMRT-Induced Bladder Wall Changes in Prostate Cancer Patients: A Relationship with Radiation Dose and Toxicity. J. Med. Imaging Radiat. Sci. **50**, 252–260, doi:10.1016/j.jmir.2018.12.002 (2019).
15. Lorenz, J. W. *et al.* Serial T2-Weighted Magnetic Resonance Images Acquired on a 1.5 Tesla Magnetic Resonance Linear Accelerator Reveal Radiomic Feature Variation in Organs at Risk: An Exploratory Analysis of Novel Metrics of Tissue Response in Prostate Cancer. Cureus **11**, e4510, doi:10.7759/cureus.4510 (2019).
16. Jeon, S. H. *et al.* Delta-radiomics signature predicts treatment outcomes after preoperative chemoradiotherapy and surgery in rectal cancer. Radiat. Oncol. **14**, 10, doi:10.1186/s13014-019-1246-8 (2019).
17. Choi, M. H. *et al.* MRI of pancreatic ductal adenocarcinoma: texture analysis of T2-weighted images for predicting long-term outcome. Abdom. Radiol. **44**, 122–130, doi:10.1007/s00261-018-1681-2 (2019).
18. Gong, X. Q. *et al.* Progress of MRI Radiomics in Hepatocellular Carcinoma. Frontiers in Oncology **11**, doi:10.3389/fonc.2021.698373 (2021).

19. Fave, X., Zhang, L. & Yang, J. Delta-radiomics features for the prediction of patient outcomes in non–small cell lung cancer. Sci Rep **7**, 588 (2017).
20. Boldrini, L. *et al.* Delta radiomics for rectal cancer response prediction with hybrid 0.35 T magnetic resonance-guided radiotherapy (MRgRT): a hypothesis-generating study for an innovative personalized medicine approach. La radiologia medica, doi:10.1007/s11547-018-0951-y (2018).
21. Nasief, H. *et al.* A machine learning based delta-radiomics process for early prediction of treatment response of pancreatic cancer. npj Precision Oncology **3**, 25, doi:10.1038/s41698-019-0096-z (2019).
22. Eisenhauer, E. A. *et al.* New response evaluation criteria in solid tumours: revised RECIST guideline (version 1.1). Eur J Cancer **45**, 228–247, doi:10.1016/j.ejca.2008.10.026 (2009).
23. Collewet, G., Strzelecki, M. & Mariette, F. Influence of MRI acquisition protocols and image intensity normalization methods on texture classification. Magn Reson Imaging **22**, 81–91, doi:10.1016/j.mri.2003.09.001 (2004).
24. Haralick, R. M., Shanmugam, K. & Dinstein, I. TEXTURAL FEATURES FOR IMAGE CLASSIFICATION. Ieee Transactions on Systems Man and Cybernetics **SMC3**, 610–621, doi:10.1109/tsmc.1973.4309314 (1973).
25. Haralick, R. M. STATISTICAL AND STRUCTURAL APPROACHES TO TEXTURE. *Proc. IEEE* **67**, 786–804, doi:10.1109/proc.1979.11328 (1979).
26. Thibault, G. *et al. Texture Indexes and Gray Level Size Zone Matrix Application to Cell Nuclei Classification*. (2009).
27. Dasarathy, B. V. & Holder, E. B. Image characterizations based on joint gray level—run length distributions. Pattern Recognition Letters **12**, 497–502, doi:https://doi.org/10.1016/0167-8655(91)80014-2 (1991).
28. Amadasun, M. & King, R. Textural features corresponding to textural properties. IEEE Transactions on Systems, Man, and Cybernetics **19**, 1264–1274, doi:10.1109/21.44046 (1989).
29. Zwanenburg A, L. S., Vallières M, Löck S. Image biomarker standardization initiative. arXiv preprint arXiv:1612.07003 (2019).
30. Hastie, T., Tibshirani, R. & Friedman, J. H. *The elements of statistical learning: data mining, inference, and prediction*. (2009).
31. Cusumano, D. *et al.* Delta radiomics for rectal cancer response prediction using low field magnetic resonance guided radiotherapy: an external validation. Phys Med **84**, 186–191, doi:10.1016/j.ejmp.2021.03.038 (2021).
32. Boldrini, L. *et al.* Delta radiomics for rectal cancer response prediction with hybrid 0.35 T magnetic resonance-guided radiotherapy (MRgRT): a hypothesis-generating study for an innovative personalized medicine approach. Radiol Med **124**, 145–153, doi:10.1007/s11547-018-0951-y (2019).
33. Cusumano, D. *et al.* Delta Radiomics Analysis for Local Control Prediction in Pancreatic Cancer Patients Treated Using Magnetic Resonance Guided Radiotherapy. Diagnostics (Basel) **11**, doi:10.3390/diagnostics11010072 (2021).

34. Simpson, G. *et al.* Predictive value of 0.35 T magnetic resonance imaging radiomic features in stereotactic ablative body radiotherapy of pancreatic cancer: A pilot study. Med Phys **47**, 3682–3690, doi:10.1002/mp.14200 (2020).
35. Jeon, S. H. *et al.* Delta-radiomics signature predicts treatment outcomes after preoperative chemoradiotherapy and surgery in rectal cancer. Radiat Oncol **14**, 43, doi:10.1186/s13014-019-1246-8 (2019).
36. Randen, T. & Husoy, J. H. Filtering for texture classification: a comparative study. IEEE Trans. Pattern Anal. Mach. Intell. **21**, 291–310, doi:10.1109/34.761261 (1999).
37. Mallat, S. G. A THEORY FOR MULTIRESOLUTION SIGNAL DECOMPOSITION - THE WAVELET REPRESENTATION. IEEE Trans. Pattern Anal. Mach. Intell. **11**, 674–693, doi:10.1109/34.192463 (1989).
38. Soni, N., Priya, S. & Bathla, G. Texture Analysis in Cerebral Gliomas: A Review of the Literature. Am. J. Neuroradiol. **40**, 928–934, doi:10.3174/ajnr.A6075 (2019).
39. Chitalia, R. D. & Kontos, D. Role of texture analysis in breast MRI as a cancer biomarker: A review. Journal of Magnetic Resonance Imaging **49**, 927–938, doi:10.1002/jmri.26556 (2019).
40. Thawani, R. *et al.* Radiomics and radiogenomics in lung cancer: A review for the clinician. Lung Cancer **115**, 34–41, doi:10.1016/j.lungcan.2017.10.015 (2018).
41. Lucia, F. *et al.* Prediction of outcome using pretreatment (18)F-FDG PET/CT and MRI radiomics in locally advanced cervical cancer treated with chemoradiotherapy. Eur J Nucl Med Mol Imaging **45**, 768–786, doi:10.1007/s00259-017-3898-7 (2018).
42. Cozzi, L. *et al.* Computed tomography based radiomic signature as predictive of survival and local control after stereotactic body radiation therapy in pancreatic carcinoma. PLOS ONE **14**, e0210758, doi:10.1371/journal.pone.0210758 (2019).

Figures

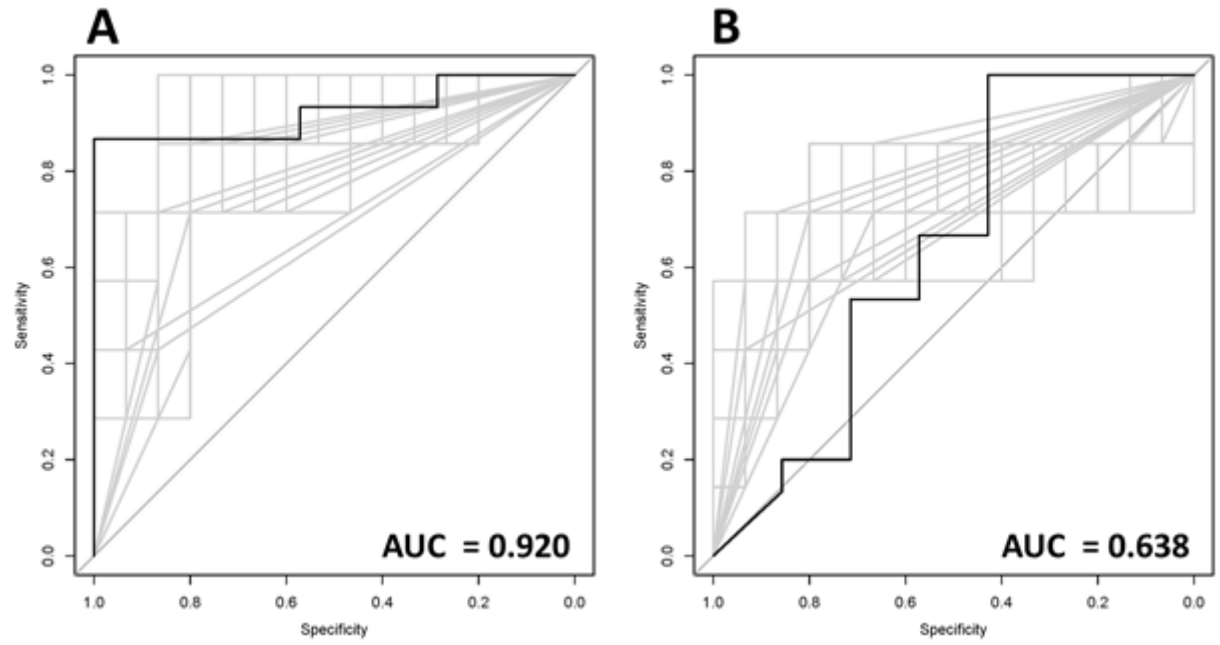

Figure 1

The bolded receive operator characteristic curve in each graph represents the random forest's estimate obtained during training for (a) BED_{20} and (b) BED_{40}. The AUC for the BED_{20} delta-radiomics features = 0.920 and the AUC for the BED_{40} was = 0.638.

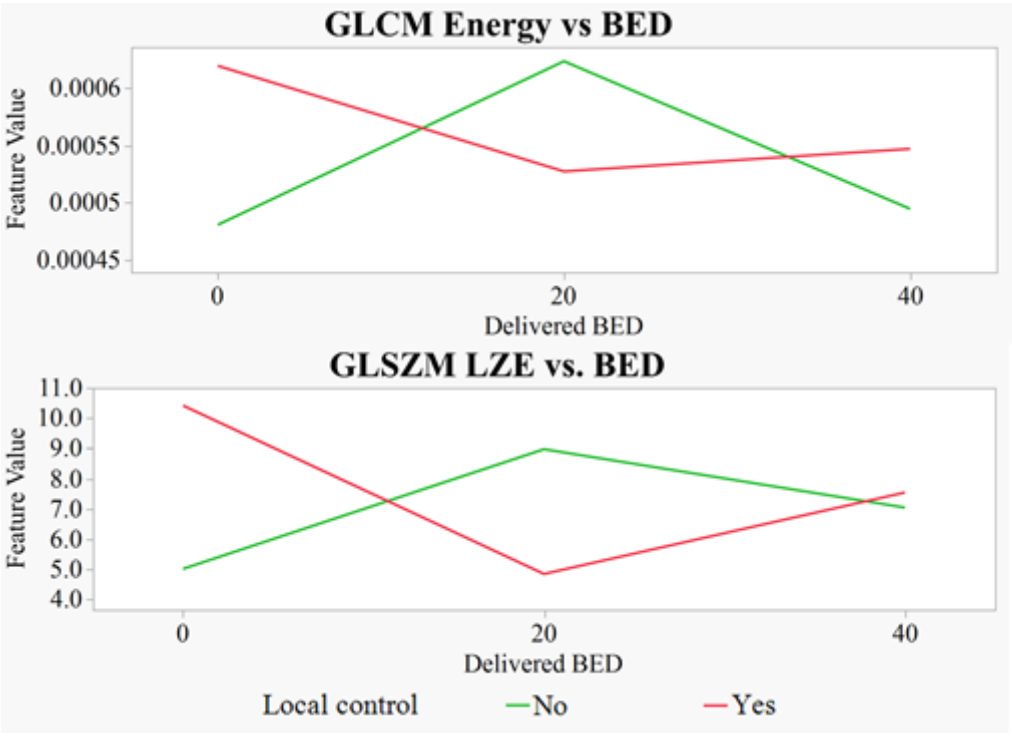

Figure 2

Mean feature values prior to delivery (BED = 0), after delivery of BED 20 Gy, and after BED 20 Gy. Both features increased for the patients with treatment response from before treatment and delivery of BED 20 Gy. Delivery of another BED 20 Gy resulted in a decrease in feature values between the BED 20 Gy and BED 40 Gy timepoints. Patients with poor treatment response demonstrated opposite trends, with an initial decrease in feature values followed by an increase by the BED 40 Gy point. BED: biologically effective dose (calculated using $\alpha/\beta = 10$), GLCM: gray level co-occurrence matrix, GLSZM: gray level size zone matrix, LZE: large zone emphasis.